The American Mineralogist, Volume 60, pages 889–897, 1975

X-Ray Topographic Study of a Topaz Crystal

MINEO ISOGAMI AND ICHIRO SUNAGAWA

Institute of Mineralogy, Petrology and Economic Geology, Tohoku University, Aoba, Sendai, Japan

Abstract

X-ray topographic studies were made of a succession of thin plates cleaved parallel to the basal plane from the bottom to the top of a prismatic crystal of topaz from a pegmatite druse in granite at Naegi District, Gifu Prefecture, Japan. Various types of contrast images, such as growth horizons, growth sector boundaries, dislocations, and inclusions were observed and interpreted. Some growth defects were correlated to optical anomalies. The contrast images vary considerably from the bottom to the top as well as from the center to the edges of the crystal. From these the growth history of the crystal was deduced as follows: (1) initial rapid growth stage; (2) layer growth stage on {001}, {110}, {111}, and {221}; (3) intermission of growth and slight dissolution by newly introduced solution; (4) final layer growth on {120}, {021}, {111}, and {221}.

Introduction

X-ray topography has been recently applied extensively for characterization of synthetic crystals, especially in the electronics industry, but not much for mineral crystals, in spite of its potential ability in elucidating growth histories. Although several important X-ray topographic studies of natural crystals have been reported, such as of diamond (Lang, 1963), fluorite (Calas and Zarka, 1973), calcite (Authier and Sauvage, 1966), quartz (Lang, 1967), *etc,* the main emphasis has been on structural imperfections rather than on growth history.

We have therefore attempted to apply X-ray topography to the study of the growth history of natural minerals. For this purpose, we prepared successive thin plates from the bottom to the top of a natural topaz crystal, and took X-ray topographs, so that the changes of various types of lattice imperfections, growth horizons, external forms, and so forth during the whole growth history of the crystal could be elucidated. We hope through this type of investigation to understand how topaz crystals nucleate and grow in cavities of pegmatites under pneumatolytic conditions. It is also expected that optical anomalies such as sector structures, which have been reported to occur commonly in topaz crystals, may be correlated to growth defects.

Natural topaz crystals have been studied by means of etch figures (Honess, 1927), optical anomalies (Yatani, Kawasaki, and Otsuki, 1901; Rinne, 1926), crystal structure (Alston and West, 1928; Pauling, 1928; Ribbe and Gibbs, 1971), optical and thermal properties (Kôzu and Ueda, 1929), twinnings and intergrowths (Gliszczcynski, 1949), and surface microtopography of crystal faces (Sasaki, 1972). X-ray topographic studies on natural topaz crystals have been reported only by Zarka (1974) and by Authier (private communication).

Sample and Experimental

The topaz crystal investigated was supplied by Dr. K. Sakurai to whom we are indebted. The crystal came from Naegi District, Gifu Prefecture, Japan, from a pegmatitic druse in the granite of Cretaceous age. Topaz crystals in this District are considered to be the latest formation of pegmatite minerals, growing most frequently on quartz and rarely on mica crystals in druses. Other associated minerals are beryl and black tourmaline, which formed earlier than topaz, having been enclosed in quartz and mica (Wada, 1904).

The crystal investigated is prismatic, 2.5 cm in length, 1.8 cm × 2.2 cm across, and is slightly brown in color and nearly transparent but heavily corroded. The crystal is bounded by well-developed *f*(021), *l*(120), *m*(110) faces, together with smaller *u*(111), *o*(221), and *d*(201) faces (Fig. 1).

Since topaz has a perfect basal cleavage, a successive series of thin plates about 0.2 mm to 1.5 mm thick were cleaved parallel to the basal plane, from the bottom to the top of the crystal. These plates were mechanically polished and then etched for about half

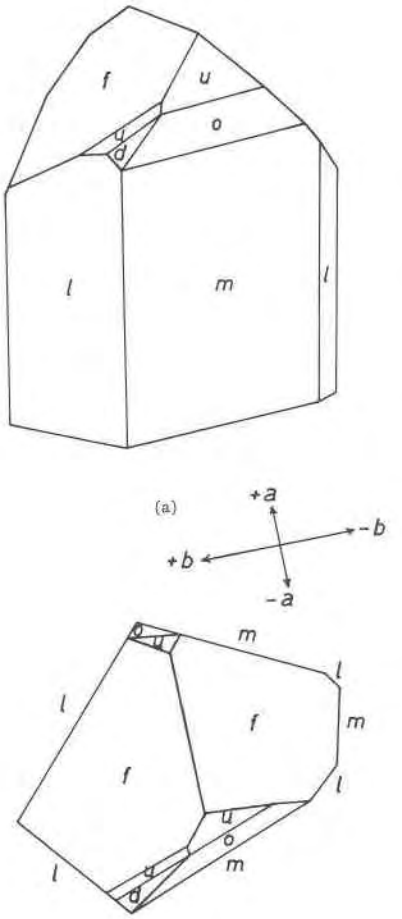

FIG. 1. Drawing of the forms present—$m\{110\}$, $l\{120\}$, $f\{021\}$, $u\{111\}$, $o\{221\}$, $d\{201\}$—on the topaz crystal studied.

an hour at temperatures around 150°-160°C in concentrated KOH solution to remove surface damage. However, it was not easy to remove completely the surface damage caused by cleaving or polishing, though this is easily discriminated from other types of defects. The plates thus obtained were numbered from $L = 0$ to $L = 8$ from the bottom to the top of the crystal.

X-ray topographs were taken by transmission, using a Rigaku Denki Lang camera. All traverse topographs were taken with Ag$K\alpha$ radiation, operating at 50 kV and 1 mA. Images were recorded on SAKURA Nuclear Plates emulsion NR-E1, 50 μ thick. Each topograph was subsequently enlarged by photographic procedure through an intermediate contrast inversion step.

Reflections of type {120} were mainly used for the investigation of growth history, because the {120} faces develop as large natural growth faces. For identification of orientations and structural defects, the *020, 040, 220,* and *111* reflections were also used.

X-Ray Topography

Various types of complicated contrast images occur on all plates investigated, from $L = 0$ to $L = 8$. Some are seen only on the lower plates, others only on the upper plates, others throughout the crystal. The lowest plate, $L = 0$, exhibits the most complicated and irregular contrast images, whereas the upper plates show more or less regular and crystallographic contrast images. The images may be classified as follows: wavy growth horizons, straight growth horizons, growth sector boundaries, dislocations, impurities, and surface damage. These will be explained separately.

Wavy Growth Horizons

Of the two types of growth horizons, wavy and straight, the wavy growth horizons are seen only on the lowest plate, $L = 0$, occurring along the marginal portions of the crystal and also from the central portion to the (120) face (Fig. 2). They consist of narrow white stripes alternating with dark wide stripes, some of which exhibit fine textures within one stripe. Therefore, they can not be related to irregular Pendellösung fringes. Although they are not straight,

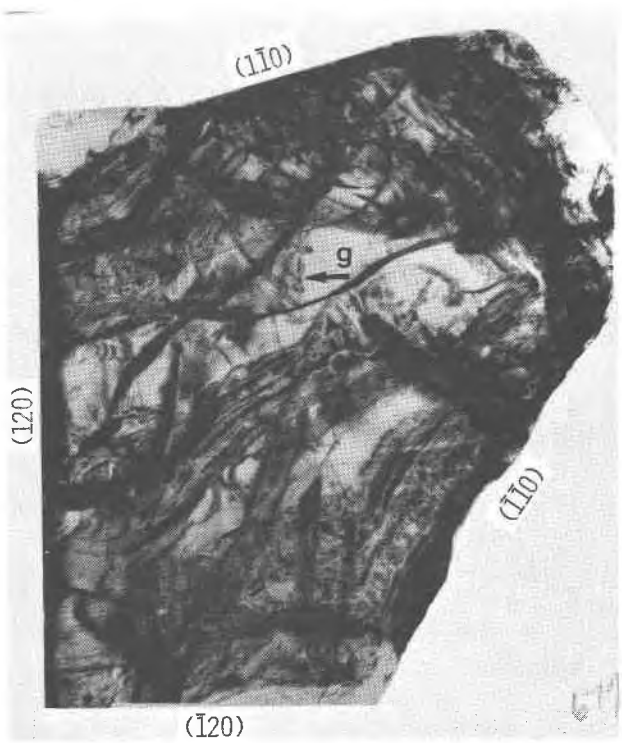

FIG. 2. X-ray topograph of the lowest plate, $L = 0$. All X-ray topographs are printed in orientations that conform to Figure 1.

their general trends are principally parallel to the {110} faces, partly to the {120} faces, except those running from the center to the (120) face. They are essentially continuous from one face to the neighboring faces, and in some cases they become almost straight (lower left, Fig. 2), when parallel to the external (120) face. Incidentally, straight growth horizons, which occur commonly on the upper plates, are entirely absent on the lowest plate, $L = 0$.

The wavy stripes nearly parallel to the {110} faces must represent initial growth horizons because they occur only at the bottom of the topaz crystal where it rests on the pre-existing minerals.

Their waviness suggests that no regular layer growth took place at this stage of growth.

The wavy growth horizons that run from the central portion to the (120) face are flanked by two clear white areas, corresponding to near perfect portions (Fig. 2). This suggests that the crystal actually consists of two crystals that coalesced in nearly parallel orientation and that the central wavy growth horizons represent the boundary between the two. Both crystals should have grown independently but in near parallel orientation in the initial stage, and then coalesced together to form an apparent single crystal of the present form. This coalescence occurred at the initial stage while the crystals were more or less in a low plateau-like form, since this sort of pattern is observed only on the plate $L = 0$, and not on the upper plates.

Straight Growth Horizons

Two types of straight stripe patterns, each trending parallel to crystallographic directions with low rational indices, are observed universally on the plates where $L = 1$ and above. One type consists of alternating dark and bright stripes having regular spacings and uniform darkness, which can be seen around the central rhombic pattern in Figure 3a. These are considered to be fringes appearing along growth sector boundaries, and will be described in the following section. The other type has irregular spacings and each stripe varies in darkness from place to place.

Typical examples of the latter type may be seen in Figure 3c, an X-ray topograph taken with *040* reflection. In this topograph, straight stripes run parallel to the intersection between the (120) or ($\bar{1}$20) faces and this slab section, as well as parallel to the ⟨010⟩ direction. The former can be traced from the lower to the upper slab sections as parallel to the external (120) and ($\bar{1}$20) faces; thus they are most probably growth horizons parallel to these faces. The growth horizons parallel to the (120) face appear in Figure 3a (*120* reflection) and disappear in 3b (*$\bar{1}$20* reflection), whereas those parallel to ($\bar{1}$20) face appear in Figure 3 b and disappear in Figure 3a.

The growth horizons parallel to ⟨010⟩ in Figure 3c are seen on both Fig. 3a and b, showing that they are not parallel to the {010} face but most probably parallel to the (021) face which develops as a large external face.

These straight growth horizons are attributed to regular layer growth. As to their nature, we do not have enough information to draw a conclusion, except that they must have been formed by changes in growth environment or growth speed. They may be concentrations of dislocations, stacking faults, inclusions, changes in d values, or localized lattice misorientations, all of which can be created by changes in growth environment or growth speed.

Growth Sector Boundaries

At the center of Figure 3a and b is clearly seen a high contrast rhombic pattern and the surrounding fringe patterns. The rhombic pattern is bounded by ⟨110⟩ directions. In Figure 3a, which is taken by *120* reflection, strong contrast images appear on [1$\bar{1}$0] and faint contrast images on [110], whereas when the **g** vector is reversed to $\bar{1}$20, contrast images are also reversed (Fig. 3b).

Figure 4 shows a series of X-ray topographs of the rhombic pattern taken with different reflections. Visibility of the rhombic pattern changes regularly according to the choice of reflections, as for dark-field electron microscope images of stacking faults. The rhombic pattern is, therefore, considered to be bounded by fault surfaces.

The fault surface indicated by A in Figures 3a and 4 runs parallel to [1$\bar{1}$0] so that the fault surface should lie on either (11l) or (11$\bar{l}$), and most probably on (111) or (11$\bar{1}$).

From the consideration of the direction of incident X-rays to the surface and the changes of the intensities of both edges of the fault image, the top and the bottom edges of the fault can be distinguished (Hirsch *et al,* 1965). It is concluded from these that the fault surface indicated as A in Figure 3 and 4 lies on the (11$\bar{1}$) and not on the other {111} faces.

The contrast of fault surface A is very faint on the topograph of 1$\bar{1}$0 reflection (Fig. 4c), and entirely invisible on the topograph of $\bar{1}$11 reflection (Fig. 4f). Since a fault may become effectively invisible if the value of $\mathbf{g} \cdot \mathbf{R}$ is very close to an integral (**g** is the

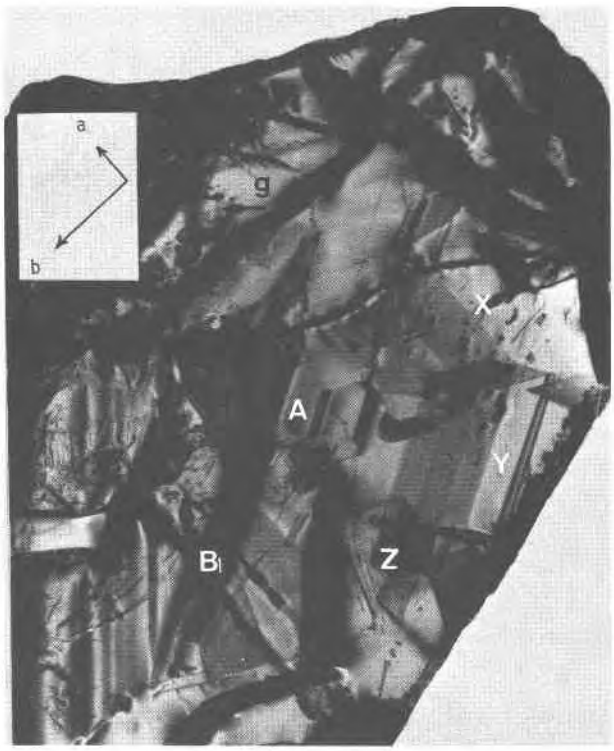

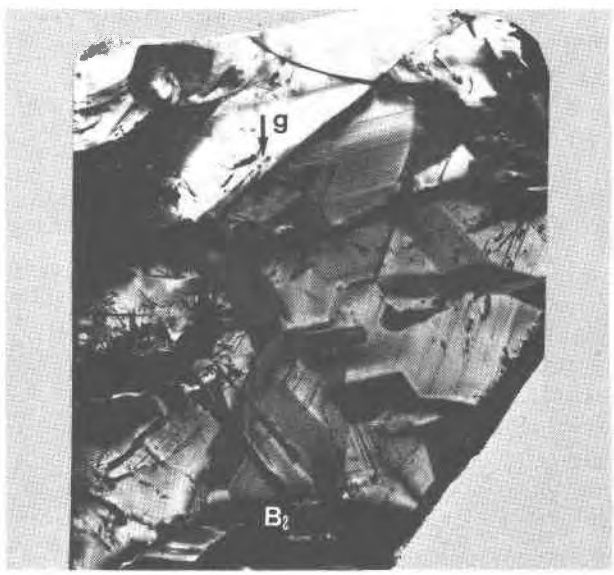

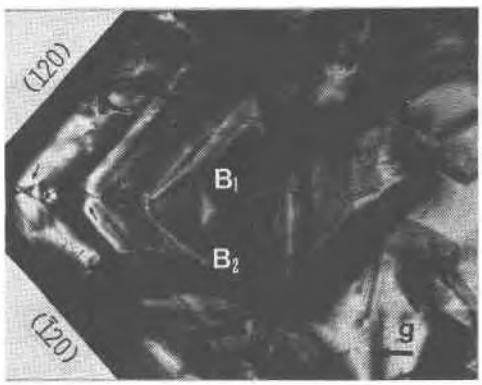

FIG. 3. X-ray topographs of plate $L = 1$. (a) *120* reflection, (b) $\bar{1}20$ reflection, (c) *040* reflection.

diffraction vector, **R** the fault vector), the vector of the fault should be $\mathbf{R} = \frac{1}{6}[211]$. It should be noted that the fault vectors $\mathbf{R} = \pm\frac{1}{3}[111]$ were not detected in this crystal, as the fault images do not vanish on {220} type reflections. It is therefore conjectured that the fault surface observed here is formed by the slip of $\frac{1}{6}\langle 211\rangle$ type on {111} planes. Since the rhombic pattern observed on X-ray topographs consists of {111} fault surfaces with fault vectors $\mathbf{R} = \frac{1}{6}\langle 211\rangle$, these fault surfaces should coincide with growth sector boundaries, perhaps between growth sectors of (001) and {111}.

Fringe patterns are seen surrounding the central rhombic pattern, as indicated by the signs X, Y, Z in Figure 3a. This sort of fringe pattern, which can be seen both under the electron microscope and X-ray topographs, may be ascribed to a grain boundary, a stacking fault, a twin boundary, or a wedge-shaped crystal. In the case of a twin boundary, the diffraction condition is, in general, satisfied only on one side of the twin plane and not on the other; thus contrast images of either side may disappear depending on different reflections. However, such a feature was not detected for any reflection. Furthermore, the angle between the plane giving rise to the fringe pattern and the crystal surface, (001), can be calculated from the width and orientation of each fringe; these results are shown in Table 1. It should be noticed that the angles do not coincide with any of the interplanar angles reported for twinning planes in topaz, *i.e.* (110) and (101), but they are consistent with angles between the slab (001) and $f\{021\}$, $u\{111\}$, or $0\{221\}$ faces. The fringes X, Y, Z are, therefore, considered to have appeared on the boundary between the (001) growth sector and {021}, $(\bar{1}\bar{1}1)$, and $(\bar{2}21)$ growth sectors, respectively. We consider that the fringes are either Pendellösung type or Moiré-type formed by the overlapping of two different growth sectors.

Defect Surfaces

In Figure 3, strong contrast images of wavy defect surfaces are seen as indicated by B_1 and B_2. The defect surface B_1 traverses from the upper central to the lower left in Figure 3a, and B_2 develops in the lower

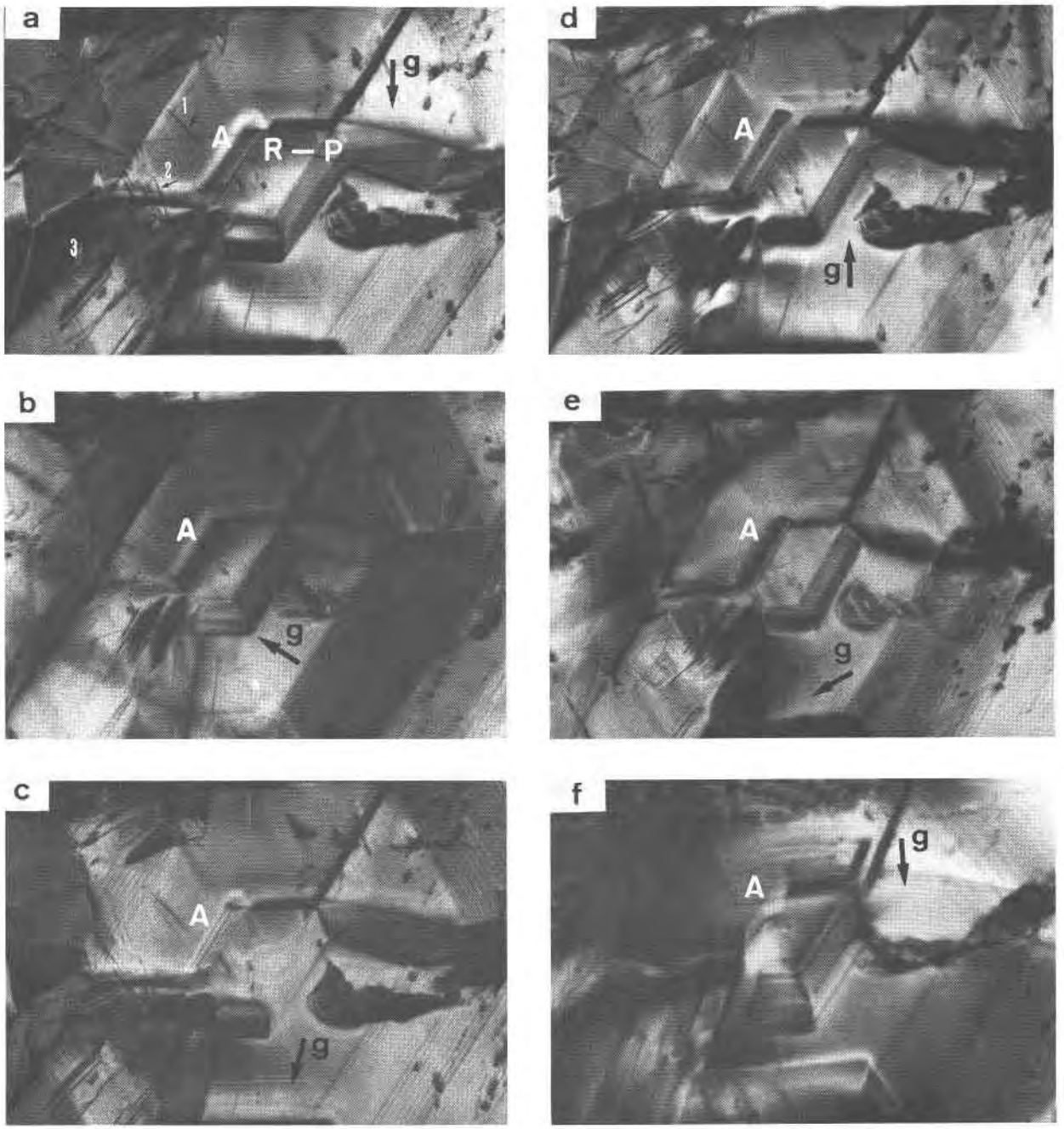

FIG. 4. Changes of contrast images of the rhombic pattern according to the reflections. (a) $\bar{2}20$, (b) 220, (c) $\bar{1}20$, (d) $2\bar{2}0$, (e) 040, (f) $\bar{1}11$.

part in Figure 3b; both B_1 and B_2 are seen in Figure 3c. These two defect surfaces can be traced from plates $L = 1$ to $L = 4$. They show more or less wavy outlines, but the striking observation is that the directions of growth horizons on opposite sides of the defect surfaces are markedly changed. This is clearly seen on the opposite sides of B_1 in Figure 3a. On the right side, the growth horizons are parallel to [010], whereas on the left side they trend parallel to the trend of (120). Furthermore, contrast images of the growth horizons are distinctly different on the opposite sides. On the right, the width of the stripes is narrow and their spacings more or less uniform, whereas on the left they are thick and irregularly

TABLE I. Calculated Angles between the Plane Giving Rise to the Fringe Pattern and the Crystal Surface (001)

Fringes	d	Observed inclination to (001)	Corresponding faces	Calculated interfacial angles with (001)
X	10.0 mm	66°20'	f(0$\bar{2}$1)	62°22'
Y	10.3 mm	65°36'	u($\bar{1}\bar{1}$1)	63°56'
Z	7.5 mm	72°57'	o($\bar{2}$21)	76°15'

Observed inclinations to (001) were calculated by the following formula;

$$\tan \alpha = t/\frac{d}{f} - t \tan \Theta$$

where α is an inclination, t thickness of the slab (1.3 mm), d magnified width of fringe pattern, f magnification (x 14.6), and Θ incident angle of X-ray beam ($2\theta(Ag K\alpha)=10.1°$).

spaced. These differences suggest that on the opposite sides of B_1 there must have been a remarkable change in growth process.

Since growth horizons seen at the lower right side of B_1 in Figure 3a are the horizons parallel to the edge of the slab along the *f*(021) face, and those on the upper left side of B_1 are the horizons parallel to the edge of the slab along the *l*(120) face, the defect surface B_1 may be the boundary surface between the growth sectors of (021) and of (120). In addition, {110} faces should also be taken into consideration. Thus, we consider that the defect surface B_1 (and also B_2 in Fig. 3b) is the boundaries formed between the earlier {110} and later {120} growth sectors, as well as between the {120} and {021} sectors. Since the defect surfaces B_1 and B_2 are wavy and curved and give stronger contrast effect than any other types of growth sector boundaries, we conjecture that there was an abrupt change of growth conditions, *i.e.*, an intermission and weak dissolution period in the transition from {110} growth to {120} growth. Since the defect surface B_1 (and also B_2), which is not on the close-packed plane, will have larger strain than the crystallographic defects developing around the central rhombic pattern, we expected that the defect might be seen as a birefringence pattern under the polarizing microscope, about which will be described later.

Dislocations

Figure 5 shows several different types of line defects, which run, in general, in straight lines, approximately normal to the growth face; curved or branched line defects are also seen. Some show wide and strong dark contrast images, others narrow and faint contrast. The former represents a bundle of dislocations, and the latter a single dislocation.

Figures 5a and b are a paired topograph taken with reflections, $\bar{2}20$ and $2\bar{2}0$. In the two circles, one may see branched dislocations, and also notice that the fringes exhibit bending at branching of dislocations. Now, the crystal structure of topaz (*Pbnm, a* 4.650 Å, *b* 8.800 Å, *c* 8.394 Å) is based on the oxygen layers alternating with the layers of composition F_2O, in the closed packed sequence ABAC, the close-packed plane being (010) (Ribbe and Gibbs, 1971). From the configuration of the oxygen layers in the crystal structure, possible Burgers' vectors of dislocations may be analyzed to be $\mathbf{b}_1 = \frac{1}{8}[101]$, $\mathbf{b}_2 = \frac{1}{8}[\bar{1}01]$, $\mathbf{b}_3 = \frac{1}{8}[10\bar{1}]$, $\mathbf{b}_4 = \frac{1}{8}[001]$, $\mathbf{b}_5 = \frac{1}{8}[100]$, and probably $\mathbf{b}_6 = \frac{1}{2}[301]$, as schematically shown in Figure 6. The related Frank's rule may be expressed as

$$\mathbf{b}_5^2 < \mathbf{b}_1^2 + \mathbf{b}_3^2 \cdots\cdots (1)$$

$$\mathbf{b}_4^2 > \mathbf{b}_1^2 + \mathbf{b}_2^2 \cdots\cdots (2)$$

If Burger's vectors of topaz are $\mathbf{b}_4 = \frac{1}{8}[001]$, $\mathbf{b}_1 = \frac{1}{8}[101]$, $\mathbf{b}_2 = \frac{1}{8}[\bar{1}01]$, it is expected from formula (2) that the $\frac{1}{8}[001]$ dislocation will split into two partial dislocations, $\frac{1}{8}[101]$ and $\frac{1}{8}[\bar{1}01]$. The branched dislocations may possibly be of this type. From the changes

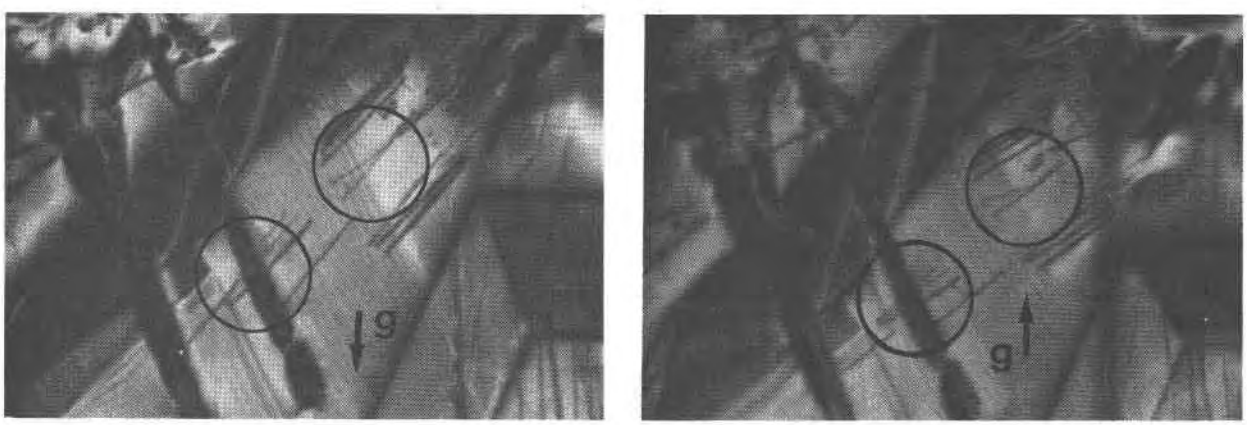

(a) (b)

FIG. 5. Paired X-ray topographs of dislocations. (a) $\bar{2}20$, (b) $2\bar{2}0$.

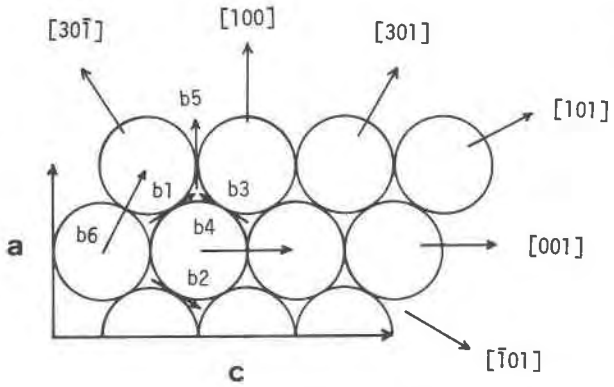

FIG. 6. Possible Burgers' vectors of dislocations in topaz.

of visibility of dislocation images depending on different reflections, the Burgers' vectors of dislocations marked as 1, 2, 3 in Figure 4 were identified to be [001], [101], and [011], respectively.

It is seen that dislocation bundles often originate from a corner of rhombic pattern or from impurities. This is clearly seen in Figures 4, 5, *etc.*

Inclusions

Inclusions appear as strong contrast images of point type or of alignment of points on X-ray topographs. These can be seen throughout the crystal, though some occur selectively. At the lower center of Figure 3a, two parallel lines of strong contrast images are seen to develop nearly parallel to the [100] direction. The lines are inclusions aligned in rows. At the left of Figure 3c, a track of dotted strong contrast images indicated by arrows are seen at the intersections of growth horizons parallel to (120) and ($\bar{1}$20).

Surface Defects

Since topaz has a hardness of 8, it is not easy to remove entirely the surface damage induced by cleaving or polishing. These appear either as irregular strong contrast images or crack lines.

Correlation between Optical Anomalies and X-ray Topographs

When a section parallel to the basal plane of topaz is observed under crossed nicols of the polarizing microscope, various crystallographic sector structures are usually observed. These optical anomalies have been studied extensively, *e.g.*, by Yatani *et al* (1901) on Japanese topaz from Naegi, Gifu Prefecture, and by Rinne on Brazilian topaz (1926). Typical examples are shown schematically in Figure 7. If one compares these with X-ray topographs, it is natural to imagine a close relation, especially between the central rhombic pattern indicated by A in Figure 7b and that on X-ray topographs. To investigate this, plates $L = 1$ and $L = 2$ were observed under the polarizing microscope. In the case of $L = 1$, no detectable sector patterns were seen under the microscope, due to the thickness of the plate. In the case of $L = 2$, which is much thinner than $L = 1$, very faint sectors were observed (Fig. 8a). The sectors, however, do not correspond to the central rhombic pattern on the X-ray topograph (Fig. 8b), but correspond to the outer strong contrast images B1 and B2, which are growth sector boundaries, representing the portions where

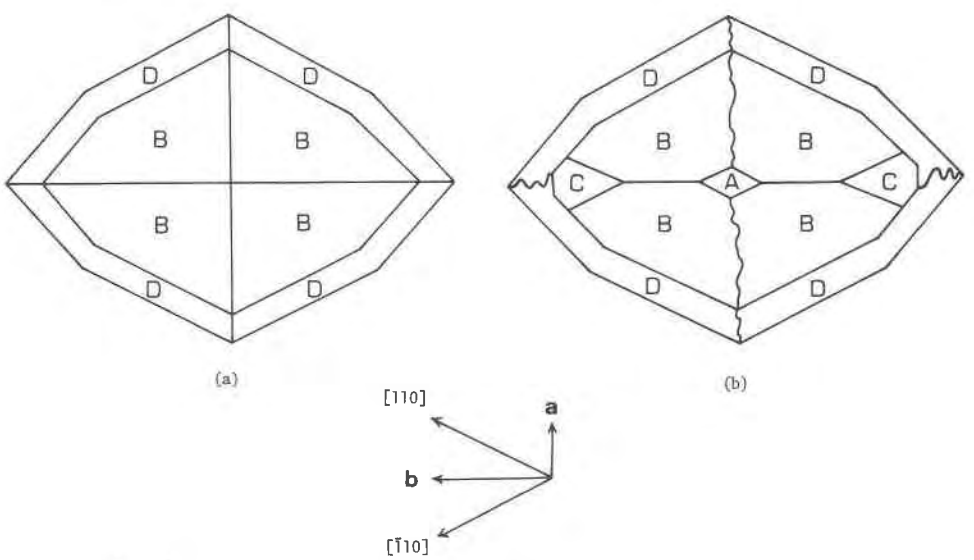

FIG. 7. Schematic drawings of optical sector patterns observed on topaz crystals.

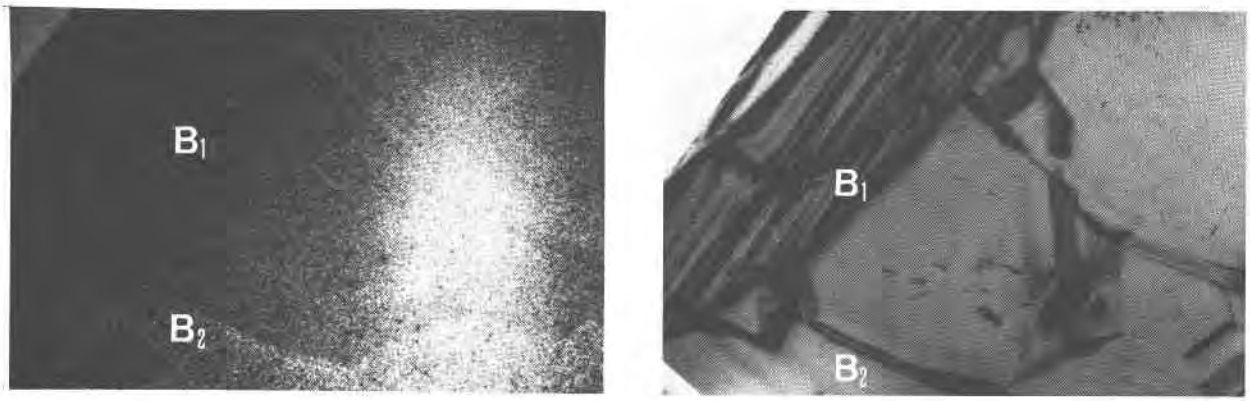

FIG. 8. Corresponding optical sector pattern (a) and X-ray topograph (b).

abrupt change in the growth process took place as described above. These observations indicate that X-ray topography is more sensitive to detect internal strains than polarizing microscopy, and that optical anomalies in topaz crystals have a direct relation to major growth defects.

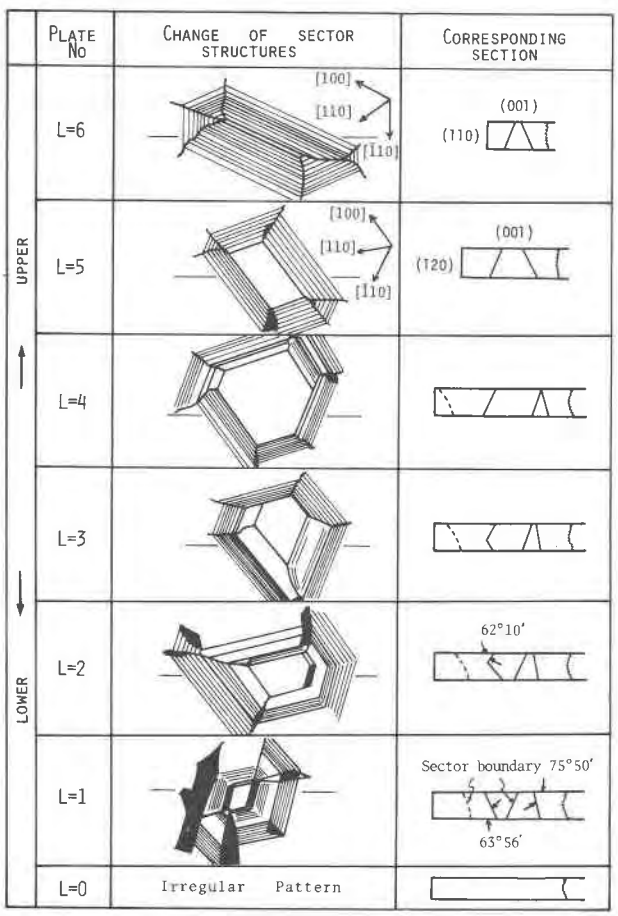

FIG. 9. Schematic drawing to show the changes of sector structures revealed by X-ray topography, from $L = 0$ to $L = 6$.

Growth History

Figure 9 shows schematically a succession of internal defects revealed by X-ray topography from the bottom to the top of the crystal. The figure is specially focused on the changes of the central rhombic pattern and the corresponding profiles. From this figure, one possible model of the whole growth history of the crystal may be elucidated as follows.

At the initial stage, growth of the topaz was rather violent, and crystallizing particles and impurities intermingled. Many crystallites were formed on the pre-existing crystals in the cavity. Some of these early crystallites coalesced to form two plateau-like crystals having the same orientation, which later joined to form a single crystal. No regular steady-state layer growth took place at this stage, and the crystal took on an irregular and uneven plateau-like form.

Then, layer growth on {001}, {110}, {111}, and probably on {221} took place and the crystal grew larger through a layer (including spiral) growth mechanism. That topaz crystals are grown by such a growth mechanism has been established by the surface microtopographic investigations of many topaz crystals from the same locality (Sasaki, 1972).

The crystal gradually changed its external form from uneven plateau to tabular, and further to short prismatic bounded by plane faces. {120} and {021} faces were not present at this stage.

Then, there was an intermission of growth. After that a new solution whose physico-chemical conditions were different was introduced into the cavity, and the crystal suffered a slight dissolution at first. Because of the change of physico-chemical conditions

of the new solution, growth took place this time mainly on the {120} and {021} faces by a layer growth mechanism. In other words, in this new solution, the growth rates perpendicular to {001} and {110} were enhanced, whereas those perpendicular to {120} and {021} were diminished. Thus, {001} and {110} faces gradually diminished in size and eventually disappeared from the crystal, whereas the {120} and {021} faces grew larger. As a result, the crystal changed its external form from tabular to short prismatic bounded by {001}, {110}, {111}, and {221} faces to slightly longer prismatic bounded mainly by {120}, {021}, {111} and {221} faces. The whole growth history was thus completed, though there was weak dissolution after the cessation of growth, which formed various etch figures on the surface.

Acknowledgment

The writers express their thanks to Dr. K. Sakurai for the specimens. Thanks are also due to Mr. T. Yasuda of Geological Survey of Japan for his guidance and help in X-ray topographic studies.

References

ALSTON, N. A., AND J. WEST (1928) The structure of topaz [$Al(F,OH)_2SiO_4$]. *Proc. Roy. Soc. A*, **121**, 358–367.

AUTHIER, A., AND M. SAUVAGE (1966) Dislocations de macle dans la calcite; interférences entre les champs d'ondes créés à la traversée d'une lamelle de macle. *J. Phys. Colloq C3, Suppl. No. 7-8*, **27**, C3-137–150.

CALAS, G., AND A. ZARKA (1973) Études des défauts de croissance dans des monocristaux de fluorite naturelle. *Bull. Soc. fr. Mineral. Cristallogr.* **96**, 274–277.

GLISZCZCYNSKI, S. VON (1949) Über gesetzmässige Verwachsungen von Topasen, I. Teil, Zwillinge, II. Teil. Koaxiale Verwachsungen. *Neues Jahrb. Mineral. Geol. Abt. A., Monatsh.* 1–23.

HACHITANI, H. S. KAWASAKI, AND F. OTSUKI (1901) Optical study of topaz from Mino district. *Chishitsu (J. Geol. Soc. Japan)*, **8**, 401 (in Japanese).

HIRSCH, P. B., A. HOWIE, R. B. NICHOLSON, D. W. PASHLEY, AND M. J. WHELAN (1965) *Electron Microscopy of Thin Crystals.* London, Butterworths, p. 229–236.

HONESS, A. P. (1927) *The Nature, Origin and Interpretation of the Etch Figures on Crystals.* John Wiley and Sons, New York. p. 148–159.

KÔZU, S., AND J. UEDA (1919) Optical and thermal studies of topaz from Naegi, Japan, *Sci. Rep. Tohoku Univ. 3*, **3**, 162–170.

LANG, A. R. (1963) Dislocations in diamond and the origin of trigons. *Proc. Roy. Soc. A*, **278**, 234–242.

——— (1967) Some recent applications of X-ray topography. *Adv. X-ray Anal.*, **10**, 91–107. Plenum Press.

PAULING, L. (1928) The crystal structure of topaz. *Proc. Nat. Acad. Sci. U.S.A.* **14**, 603–606.

RIBBE, P. H., AND G. V. GIBBS (1971) The crystal structure of topaz and its relation to physical properties of topaz. *Am. Mineral.* **56**, 24–30.

RINNE, F. (1926) Bemerkungen über optische Anomalien insbesondere des brasilianer Topaz. *Z. Kristallogr.* **63**, 236–246.

SASAKI, S. (1972) *Surface Microtopographic Study of Topaz Crystals from the Ebisu Mine, Gifu Prefecture, Japan.* Master of Sciences Thesis, Tohoku University (in Japanese).

WADA, T. (1904) *Minerals of Japan.* Tokyo. p. 89–103.

ZARKA, P. A. (1974) Etude des défauts dans des monocristaux naturels de topaze. I. Observation des dislocations. *J. Appl. Crystallogr.* **7**, 453–460.

Manuscript received, August 5, 1974; accepted for publication, March 14, 1975.